

## Resonance frequency and Q factor mapping by ultrasonic atomic force microscopy

著者	辻 俊宏
journal or publication title	Applied Physics Letters
volume	78
number	13
page range	1939-1941
year	2001
URL	<a href="http://hdl.handle.net/10097/35042">http://hdl.handle.net/10097/35042</a>

doi: 10.1063/1.1357540

# Resonance frequency and Q factor mapping by ultrasonic atomic force microscopy

Kazushi Yamanaka,<sup>a)</sup> Yoshiki Maruyama, and Toshihiro Tsuji  
*Department of Materials Processing, Tohoku University, Aoba 02, Sendai 980-8579, Japan*

Keiichi Nakamoto  
*JEOL Limited, 1-2 Musashino 3-Chome Akishima, Tokyo, 196-8554, Japan*

(Received 23 October 2000; accepted for publication 29 January 2001)

We developed an improved ultrasonic atomic force microscopy (UAFM) for mapping resonance frequency and Q factor of a cantilever where the tip is in linear contact with the sample. Since the vibration amplitude at resonance is linearly proportional to the Q factor, the resonance frequency and Q factor are measured in the resonance tracking mode by scanning the sample in the constant force mode. This method enables much faster mapping of the resonance frequency and Q factor than the previous one using a network analyzer. In this letter, we describe the principle and instrumentation of the UAFM and show images of carbon-fiber-reinforced plastic composites. © 2001 American Institute of Physics. [DOI: 10.1063/1.1357540]

It has been established that ultrasonic atomic force microscopy (UAFM)<sup>1</sup> can realize reliable measurement of stored and loss moduli<sup>2</sup> by recording the spectra of deflection vibration of a cantilever.<sup>3</sup> The stored modulus can be calculated using the resonance frequency obtained from the peak frequency of a spectrum,<sup>1,3</sup> and the loss modulus is calculated using the Q factor defined as the ratio of the peak frequency to its width.<sup>3-5</sup> For more complete analysis, the torsion vibration can be used to separate Young's modulus, the shear modulus, and Poisson's ratio.<sup>3,6</sup>

However, measurement of spectra takes a long time (typically 5 s for one point for an average of 10 times). Consequently, mapping of the resonance frequency and the Q factor takes a very long time (~91 h for a 256×256 pixel image). Recently, Kobayashi and co-workers proposed a resonance-tracking scheme to reduce the time required for mapping the resonance frequency,<sup>7</sup> but did not realize the Q factor mapping. Nevertheless, if we use the analytical relationship between the peak height of resonance and the Q factor obtained by the theory of UAFM,<sup>1,3,5,8</sup> we should be able to measure the Q factor from the vibration amplitude at resonance. Based on this idea, we developed a UAFM for mapping both the resonance frequency and Q factor of the sample. Similar technique has been reported in the field of macroscopic contact acoustic impedance measurement.<sup>9</sup> After describing the principle and instrumentation, we present clear images of carbon-fiber-reinforced plastic (CFRP) composites.

In a model of UAFM cantilever with distributed mass, the slope of the cantilever is given by<sup>1,5</sup>

$$V(x) = \frac{\partial z(x)}{\partial x} = (u_0/2) \frac{b}{L} e^{i\omega t} \left[ \sinh b \frac{x}{L} - \sin b \frac{x}{L} - B(\omega) \times \left( \sin b \frac{x}{L} + \sinh b \frac{x}{L} \right) + D(\omega) \left( \cos b \frac{x}{L} - \cosh b \frac{x}{L} \right) \right],$$

$$B(\omega) = - \frac{SS_h + a(CC_h + SC_h)}{(1 + CC_h) + a(CC_h - SC_h)}, \quad (1)$$

$$D(\omega) = \frac{CS_h + SC_h + 2aCC_h}{(1 + CC_h) + a(CC_h - SC_h)},$$

where  $z$  is the deflection of cantilever,  $u_0$  is the vibration amplitude of cantilever base,  $\omega$  is the angular frequency,  $L$  is the length of the cantilever, and  $S = \sin b$ ,  $S_h = \sinh b$ ,  $C = \cos b$ ,  $C_h = \cosh b$ ,  $a = -1/b^3(3s/k + i\sqrt{3}\Gamma b^2)$ ,  $b = 3^{1/4}\sqrt{\Omega}$ . The factor  $\Omega = \omega/\sqrt{k/M}$  is the normalized frequency and  $\Gamma = \gamma/\sqrt{Mk}$  is the normalized damping coefficient, where  $M$  is the mass of cantilever,  $k$  is the cantilever stiffness,  $s$  and  $\gamma$  are the contact stiffness and damping coefficient between tip and sample. Because the slope is proportional to the signal measured by optical-deflection AFM, Eq. (1) is an analytical expression of the UAFM spectrum at a given location  $x$  of the laser beam spot.

Figure 1 shows spectra calculated using Eq. (1) with  $\Gamma \equiv \gamma/\sqrt{Mk} = 0.5, 1, 2, 5,$  and  $10$  and  $s/k = 200$ , for the laser beam spot at the end of cantilever ( $x = L$ ). The Q factor is

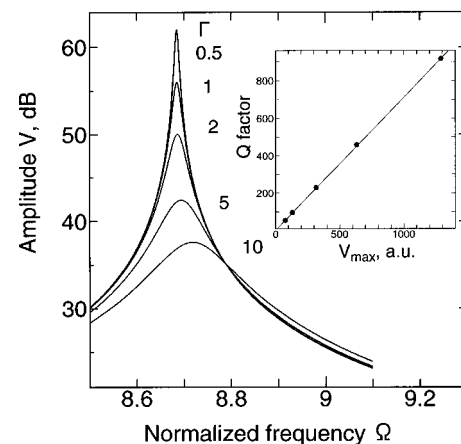


FIG. 1. Relation between the Q factor and the maximum peak height  $V_{\max}$  of a peak formed around  $\Omega \approx 0.87$  when and  $s/k = 200$ . Five different values of  $\Gamma \equiv \gamma/\sqrt{Mk}$  were assumed (0.5, 1, 2, 5, and 10).

<sup>a)</sup>Electronic mail: yamanaka@material.tohoku.ac.jp

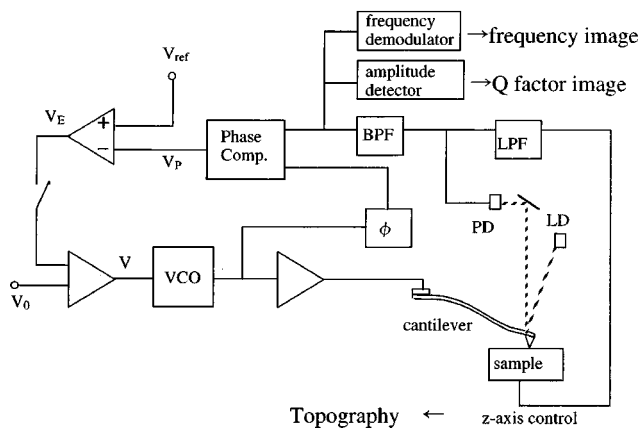


FIG. 2. Block diagram of the UAFM for resonance frequency and Q factor mapping.

calculated as the ratio of peak frequency  $\Omega_0$  to the 3 dB width  $\Delta\Omega$ . Inset of Fig. 1 shows the relation between the Q factor and the peak height of resonance  $V_{\max}$ , showing clear linearity between them. Though the linearity is an approximate relation, it holds over a reasonably wide range of normalized damping coefficient  $\Gamma$ . For example, the ratio between the Q factor and the maximum peak height  $V_{\max}$ ,  $Q/V_{\max}$ , remains almost constant (0.413–0.422) over a range of  $\Gamma$  from 0.1 to 10.0 for the normalized contact stiffness  $s/k$  of 200. For  $s/k$  larger than 200, the variation of  $Q/V_{\max}$  is even smaller. Thus, the peak height of resonance can be employed as a measure of the Q factor. The analysis can be further improved by considering the lateral stiffness,<sup>5</sup> tilt of the cantilever<sup>8</sup> and shape of the tip.<sup>10</sup>

The contribution to the Q factor in this model is from the internal friction of the sample and from the water or contaminant film on the sample. Although other factors such as the air damping, clamp of cantilever base to the ultrasonic transducer, and defects within the cantilever change the Q factor, their effect is usually small or uniform, and therefore, does not significantly affect the contrast in the image.

In the present instrumentation, the mapping of resonance frequency and Q factor is realized by the phase-locked loop circuit depicted in Fig. 2, where the cantilever vibration is excited by a voltage-controlled oscillator (VCO). The input voltage  $V$  of the VCO is adjusted to realize resonance when

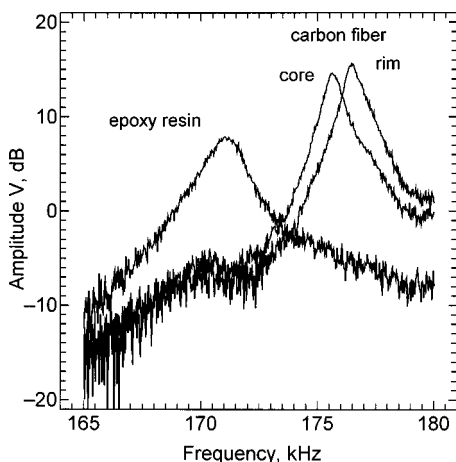


FIG. 3. Typical power spectra of cantilever deflection vibration for the carbon fiber and epoxy resin on a cross section of CFRP.

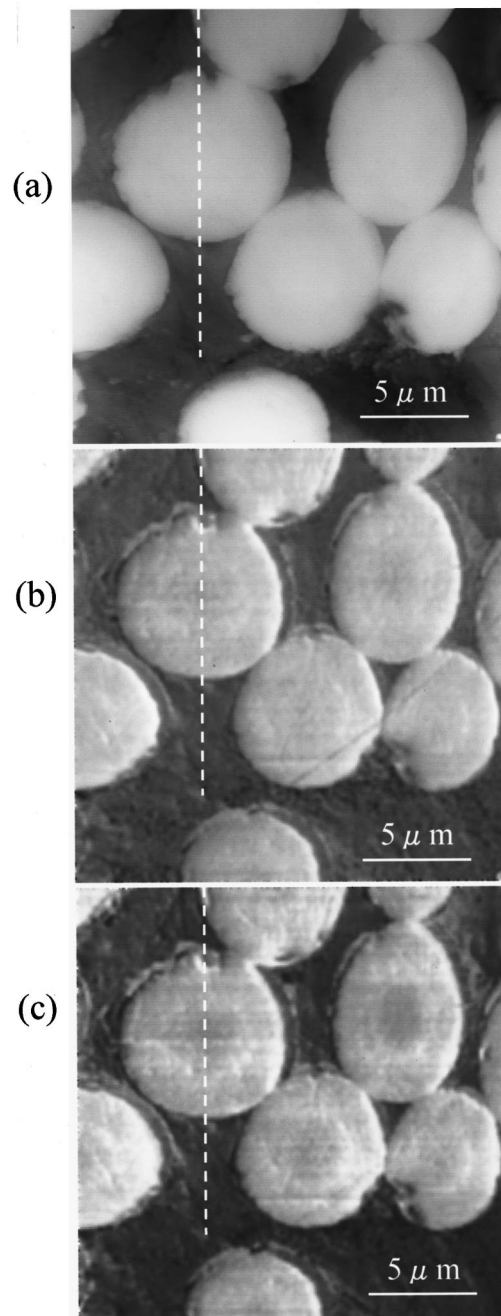


FIG. 4. Images of CFRP. (a) Topography (maximum height difference of 500 nm). (b) Resonance frequency image with a gray scale from 170 to 180 kHz. (c) Q factor image with a gray scale from 70 to 250.

the tip is in contact with the sample. Then, the cantilever deflection signal detected by the photodiode is split into two parts and one part is low-pass filtered to control the  $z$  position of the sample. The other part is band-pass filtered and its phase is compared with that of the VCO output signal. The phase difference between them is adjusted with a variable phase shifter  $\phi$  to equate the phase comparator output  $V_p$  to a reference voltage  $V_{\text{ref}}$ .

After connecting the switch, we start raster scanning of sample. If the resonance frequency is changed, the phase signal is also changed. Then, the output  $V_E$  of the error amplifier caused by the phase change is added to the VCO input in order to recover the resonance. In this manner, the cantilever is always vibrated at the resonance frequency and the vibration amplitude represents the Q factor.

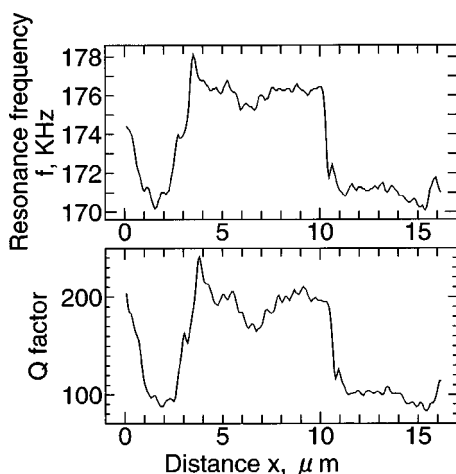


FIG. 5. Profiles of resonance frequency and Q factor obtained along the vertical lines in Fig. 4.

Whereas the resonance frequency tracking described above is similar to that of the frequency modulation mode of noncontact AFM (NC-AFM),<sup>11</sup> the vibration amplitude of the cantilever is quite different. Although it is very large ( $>10$  nm) in NC-AFM, it should be small ( $<1$  nm) in UAFM,<sup>3</sup> in order to keep the tip always in linear contact with the sample, namely the contact stiffness  $s$  should not deviate from its static value. Thus, we should carefully control the driving power of the cantilever in UAFM. To determine the optimum driving power, we monitor the vibration spectrum and find the largest possible power where the spectrum still remains symmetrical and sharp, immediately before becoming asymmetrical and broad.<sup>3</sup> Thus, both a good signal-to-noise ratio and linear contact are realized.

As an application, we imaged a carbon fiber and epoxy resin in a CFRP, at a contact force of 200 nN, using a diamond-coated silicon tip. The cantilever had a stiffness of 5 N/m and length of 0.45 mm. The vibration amplitude and phase spectra, when the piezoelectric transducer at the base of the cantilever was driven at a power of  $-35$  dBm ( $10^{-3.5}$  mW), are shown in Fig. 3. The resonance frequency increased from 38.5 kHz at free resonance to 176 kHz for the carbon and 171 kHz for the epoxy. The Q factors were 180–200 for the carbon and 100–110 for the epoxy. The peak for both the carbon and epoxy had a symmetrical shape, indicating the linear contact<sup>3</sup> at this driving power for the particular transducer used. It should be noted that we obtained the non-linearity at power levels above  $-25$  dBm.

Figures 4(b) and 4(c) are the resonance frequency and Q factor images obtained at a contact force of 200 nN corresponding the topography in Fig. 4(a). Conversion from the maximum peak height to the Q factor was experimentally performed using power spectra obtained at the carbon and epoxy area such as those shown in Fig. 3.

The images in Figs. 4(b) and 4(c) showed that epoxy was much softer and more viscous than the carbon. Within the carbon and epoxy areas, the brightness was almost uniform. However, we noted a small but reproducible variation within the carbon area. As shown in the frequency and Q factor profiles in Fig. 5 obtained along the vertical lines in Fig. 4, the resonance frequency at the core was lower than that at the rim by 0.5–1 kHz. Similarly, the Q factor at the core was lower than that at the rim by 20–40. These differences are probably due to the radial difference in the degree of stabilization during heat treatment, an important parameter for achieving high strength.<sup>12</sup> Although the qualitative difference has been indicated in a previous UAFM image,<sup>6</sup> a quantitative mapping was carried out for the first time in this study.

In conclusion, we developed an improved UAFM, where the resonance frequency and Q factor at a local area in the sample are mapped at a reasonable speed, by tracking the resonance and measuring the frequency and amplitude of cantilever vibration.

This work was supported by the Grant-in-Aid for Scientific Research (No. 10450015), and by the Grant-in-Aid for COE Research (No. 11CE2003), The Ministry of Education, Science, Sports and Culture.

- <sup>1</sup>K. Yamanaka and S. Nakano, *Jpn. J. Appl. Phys., Part 1* **35**, 93 (1996).
- <sup>2</sup>S. P. Timoshenko and J. N. Goodier, *Theory of Elasticity* (McGraw-Hill, London 1970).
- <sup>3</sup>K. Yamanaka, A. Noguchi, T. Tsuji, T. Koike, and T. Goto, *Surf. Interface Anal.* **27**, 600 (1999).
- <sup>4</sup>U. Rabe, K. Jansen, and W. Arnold, *Rev. Sci. Instrum.* **67**, 3281 (1996).
- <sup>5</sup>O. Wright and N. Nishiguchi, *Appl. Phys. Lett.* **71**, 626 (1997).
- <sup>6</sup>K. Yamanaka and S. Nakano, *Appl. Phys. A* **66**, S313 (1998).
- <sup>7</sup>K. Kobayashi, H. Yamada and K. Matsushige (unpublished).
- <sup>8</sup>U. Rabe, J. Turner, and W. Arnold, *Appl. Phys. A* **66**, S277 (1998).
- <sup>9</sup>R. Aoyagi and H. Shimizu (unpublished).
- <sup>10</sup>K. Yamanaka, A. Noguchi, T. Tsuji, T. Koike, and T. Mihara, *Rev. Sci. Instrum.* **71**, 2403 (2000).
- <sup>11</sup>F. J. Giessible, *Science* **267**, 67 (1995).
- <sup>12</sup>K. Morita, H. Miyachi, K. Kobori, and I. Matsubara, *High Temp.-High Press.* **9**, 193 (1977).